STUDY OF FATIGUE CRACK INITIATION IN ROUGH SURFACES USING THE FINITE ELEMENT METHOD AND MEASURED SURFACE TOPOGRAPHY

Sigmund Kyrre Ås[1], Bjørn Skallerud[1], Bård W Tveiten[2], Børge Holme[2]
[1]Department of Structural Engineering, Norwegian University of Science and Technology
[2]SINTEF Materials Technology
7491 Trondheim, Norway
sigmund.kyrre.as@ntnu.no

Abstract

Surface roughness is known to have great influence on fatigue life. The traditional approach is to relate the average roughness to the endurance life through a material parameter such as ultimate tensile strength. Such approaches have however shown a large degree of scatter, indicating that this approach is insufficient for relating surface topography to fatigue strength. This is the motivation for the current research, where surface roughness is modelled by finite elements obtained from measured topography. The results can be used directly in fatigue life prediction or as a foundation for evaluating and developing prediction methods. An aluminium alloy used in a wrought automotive front wheel suspension arm is used for testing and evaluation.

Introduction

Failure from cyclic loading occurs when a fatigue crack has grown large enough so that the remaining cross section cannot support the applied load. While the time to initiate a small crack of approximately 1 mm length can be determined from surface stress or strain, the propagation of larger cracks require assumptions about crack shape and component geometry. For small components such as automotive suspension arms, most of the time to failure is spent in crack initiation, thus a conservative approach is to denote the component as failed when a crack has initiated. Results from elastic finite element analysis (FEA), which is used in dynamic simulations, can therefore be used for fatigue life prediction. Surface roughness introduces microscopic stress raisers that reduce the crack initiation stage considerably compared to smooth specimens. The aim of this research is to quantify this effect by measurements, and develop methods for fatigue life prediction of components with rough surfaces.

Fatigue life prediction of rough surfaces has traditionally been considered by means of a surface correction factor that reduces the endurance life compared to that of a smooth surface. Surface factors are defined according to the machining process such as grinding, forging and polishing. Within each category, surface measurements give a quantity such as average roughness R_a, maximum peak-to-valley height R_y and 10-point roughness R_z:

$$R_a = \frac{1}{L}\int_0^L |z|dx \qquad R_y = \left|z_{\max} - z_{\min}\right| \qquad R_z = \frac{1}{5}\left[\sum_{i=1}^{5}(z_i)_{\max} + \sum_{j=1}^{5}(z_j)_{\min}\right] \tag{1}$$

L is the measured length, z is the recorded profile and i and j denote the highest peaks and lowest valleys respectively. A surface factor is found by regression with one of these

parameters, which provide an empirical fit to the observed reduction in endurance life. This is not a very flexible approach, since a large amount of testing is required to establish the relation for different surface finishes, even for a single alloy. Furthermore, the *R*-parameters are not reliable measures of surface roughness since the shape and distribution of pits and grooves are not considered.

The asperities that constitute surface roughness can be treated as microscopic notches by introducing a stress concentration factor $K_t=\sigma/\sigma_{\text{nom}}$, where σ is the stress in the notch root and σ_{nom} is the nominal stress for the cross section. Neuber [1] proposed an expression for the stress concentration factor imposed by roughness as follows:

$$K_t = 1 + 2\sqrt{\lambda \frac{R_z}{\rho}}, \tag{2}$$

where ρ is the asperity root radius and λ is the ratio between spacing and depth of the asperities. The expression then predicts less K_t for closely spaced asperities, but the actual value of λ is hard to define for generic surface textures. Arola and Williams [2] therefore suggested the following expression for the stress concentration factor:

$$K_t = 1 + 2\frac{R_a R_y}{\rho R_z}, \tag{3}$$

where the dependent parameters as given in Eq. 1 are more easily quantifiable.

In the current research, K_t is found from linear elastic FEA of the surface topography. In addition, stress gradients and principal stresses and strains can be evaluated and compared to elastic-plastic FEA. While this may provide valuable insight into the fatigue processes at microscopic notches, a fatigue assessment method should be based on a linear elastic solution in order to be of general use.

Experimental

Smooth and rough cylindrical specimens are used for fatigue testing. The material used in this study is a 6082.52-T6 aluminium alloy. Test specimens as shown in Figure 1 have been extracted from both the extruded billet material and at various locations in the forged components. Due to the expected variability in the forged specimens, testing and preliminary fatigue life prediction have been performed on the extruded specimens.

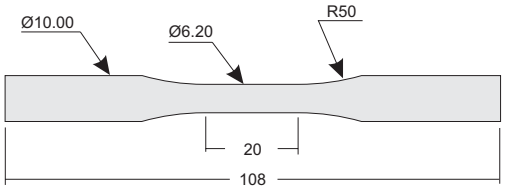

Figure 1: Test specimen geometry. [mm]

Fatigue testing

High cycle fatigue (HCF) testing is done under load control with a load ratio of R=-1 and a frequency of 15 to 20 Hz. Low cycle fatigue (LCF) testing is done at strain control with a nominal strain rate of 0.4 %/s and a strain ratio of R_ε=-1. Figure 2 shows the total strain amplitude versus cycles to failure for both HCF and LCF. Also shown is the strain life curve where the parameters σ'_f, ε'_f, b and c are found by least squares regression.

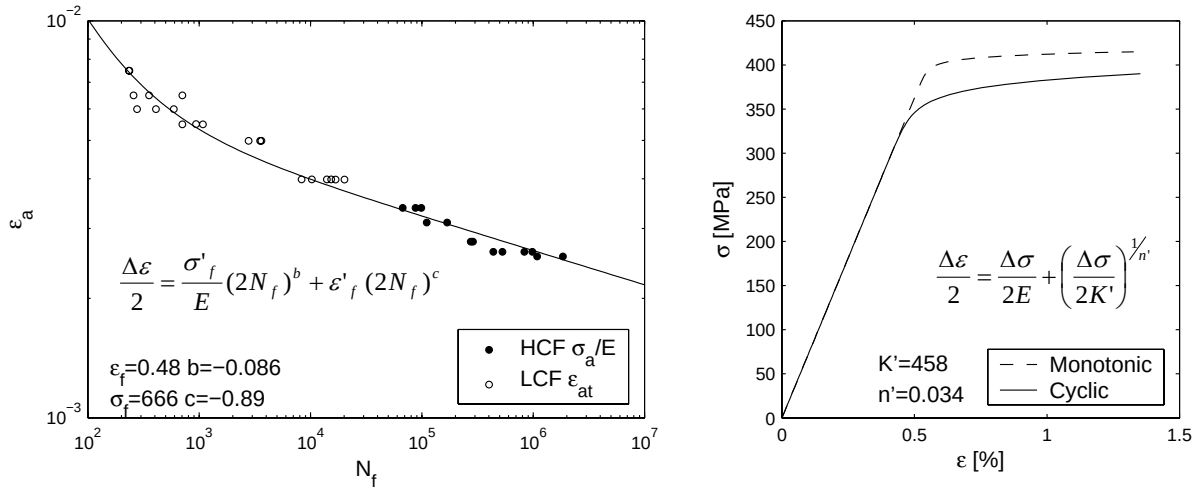

Figure 2: The strain life curve and the stress-strain response for the alloy.

The material's cyclic stress-strain response shown to the right is determined by incremental step tests and checked against the half life values of stress and strain in the LCF results.

Surface roughness is created with emery paper of various coarseness. The specimens are rotated in a lathe, while an arm and lever with emery paper is pressing against the mid-section of the specimen. This produces circumferential grooves in a repeatable way, and allows the specimens to be modelled by axi-symmetric finite elements. The average roughness R_a ranged from 3.3 to 9.3 μm and maximum peak-to-valley height R_y ranged from 21 to 75 μm.

Surface measurement

The rough specimens are measured using a white light interferometer (WLI), of the type Wyko NT2000. Three-dimensional topography is obtained by moving the objective towards the surface where the heights of areas with constructive interference are recorded. The resolution is typically 3 nm in the vertical direction and 1 μm in the lateral directions. Topography measurements using WLI have shown to be more accurate than stylus instruments [3], and it is also a much faster technique, giving 3D topography in a matter of seconds. The specimens are placed on a table that can be controlled by a computer to move in the two horizontal axes. Large areas can therefore be automatically measured by scanning several small areas and stitching them together. The cylindrical specimens are measured along the mid-section at four angular positions to capture variations around the circumference. Using a sampling interval of 3 μm, about 20 scans are needed to cover the length of the mid-section.

Finite element analysis

The 2D profile is extracted from the 3D measurements by averaging a 300 μm wide band along the centre of the measurements. The profile geometry is constructed from the sample points by piecewise cubic Bézier interpolation in order to avoid singularities associated with corners in a linear interpolation. The surface is defined by

$$\mathbf{r}_i(t) = (1-t)^3\mathbf{p}_i + 3t(1-t)^2\mathbf{b}_i + 3t^2(1-t)\mathbf{c}_i + t^3\mathbf{p}_{i+1} \quad t \in [0,1], \tag{4}$$

where $\mathbf{r}_i$ is the position vector for the spline segment i between sample points $\mathbf{p}_i$ and $\mathbf{p}_{i+1}$ as shown in Figure 3a. The control points $\mathbf{b}_i$ and $\mathbf{c}_i$ are chosen so that spline $\mathbf{r}_i$ and $\mathbf{r}_{i-1}$ have the same gradient $\mathbf{k}_i$ in $\mathbf{p}_i$:

$$\mathbf{k}_i = \frac{\mathbf{p}_{i+1} - \mathbf{p}_{i-1}}{\left|\mathbf{p}_{i+1} - \mathbf{p}_{i-1}\right|}. \tag{5}$$

The locations for the control points are then found from the sample points and their respective gradients:

$$\mathbf{b}_i = \mathbf{p}_i + \alpha\mathbf{k}_i, \quad \mathbf{c}_i = \mathbf{p}_{i+1} - \alpha\mathbf{k}_{i+1}, \quad \alpha = \tfrac{1}{3}\left|\mathbf{p}_{i+1} - \mathbf{p}_i\right|. \tag{6}$$

The factor α determines the distance from the sample points to the control points. Using the above value "divides" the spline in approximately three equal parts, which produces the most natural guess for the real surface between sample points. In Figure 3b, a solid line shows the Bézier interpolation between the WLI samples shown as dots.

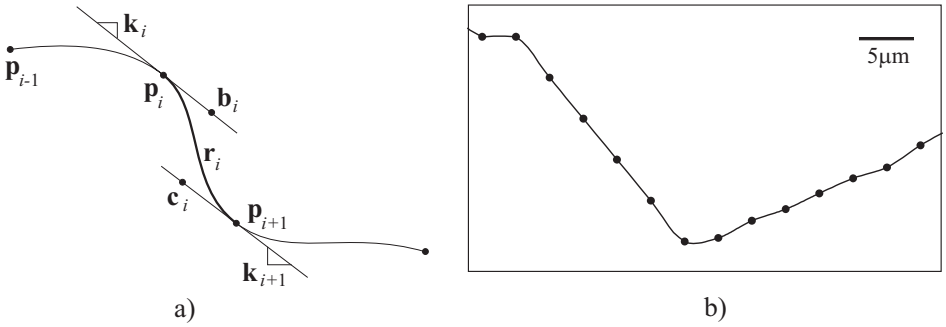

Figure 3: a) Bézier interpolation between sampled points $\mathbf{p}_i$ and $\mathbf{p}_{i+1}$ to obtain the spline $\mathbf{r}_i$. b) Interpolated profile for a specimen where the WLI samples are shown as dots.

The profiles are stored in a MATLAB database and FE meshing and calculations are done in the MATLAB toolbox FEMLAB, whereby the whole procedure from reading WLI data to extraction of stress concentration factors can be automated by MATLAB scripts. FEMLAB has internal support for Bezier splines, allowing the sample points and control to completely describe the geometry. The adaptive meshing routine can then create finer and coarser mesh depending on the curvature of the surface profile A unit tensile stress is applied to the cross section, which gives the stress concentration factor as the linear elastic solution of axial stress in the root of all notches. Axi-symmetric triangular elements with quadratic shape functions are used.

The material is assumed to be isotropic and homogenous. The smallest elements are in fact smaller than the grain size of the material, which is around 20 μm as observed in scanning electron microscope (EBSD). Hence we are on the boundary of validity for continuum mechanics, and microstructure should at some stage be accounted for.

Fatigue life prediction

The fatigue life prediction follows the strain life approach used for notched geometries. Surface asperities are treated as microscopic notches, where elastic stresses and strains are converted to local plastic stresses and strains in the notch root. Different methods can be used for this conversion, depending on the stress state in the notch root and the applied loading. The most well known approach is that due to Neuber [4], which relates nominal elastic values to notch root stress and strain as $\varepsilon\sigma = K_t^2\varepsilon_n^2 E = C$, where C is a constant and ε_n is nominal

elastic strain. Plane stress is assumed in this analysis, which can be shown is not the case for a circumferentially notched bar. A method for general stress states is outlined in the subsequent section.

It is well known that K_t gives very conservative results when used in fatigue life prediction directly. A fatigue concentration factor has therefore been defined as:

$$K_f = \frac{\Delta\sigma(N_f)}{\Delta\sigma_{nom}}, \tag{7}$$

where $\Delta\sigma_{nom}$ is the nominal stress for the notched specimen failing at N_f cycles, and $\Delta\sigma(N_f)$ is the stress range evaluated from the fatigue life curve. K_f is related to K_t by the notch sensitivity:

$$q = \frac{1-K_f}{1-K_t}. \tag{8}$$

This parameter is known to vary with material and notch geometry. Several expressions for this dependence have been proposed. They are all semi-empirical equations which try to account for the material volume influenced by the notch; a sharp notch will have a steep stress gradient into the material, thus the volume of elevated stress will be smaller than for a blunt notch. Neuber [1] and Peterson [5] among others have tried to relate q to the notch root radius in addition to a material parameter. In a previous work [6], Neuber's expression for K_f was successfully applied for predicting fatigue in the HCF range. For a random surface topography, however, the notch root radius is hard to define. Based on a large amount of empirical data, Siebel and Stieler [7] expressed K_t by the relative stress gradient:

$$K_f = \frac{K_t}{1+\sqrt{c\chi}}, \tag{9}$$

where, for loading in the z direction using cylindrical coordinates (z,θ,r), the relative stress gradient is defined from the axial stress σ_z as:

$$\chi = \frac{1}{\sigma_{notch}}\left(\frac{\partial\sigma_z}{\partial r}\right)_{r=0}, \tag{10}$$

where the peak stress in the notch root is σ_{notch}. The gradient can be extracted from the FE solution where the strain-displacement relations assuming small strains are:

$$\varepsilon_r = \frac{\partial u}{\partial r}, \quad \varepsilon_\theta = \frac{u}{r} = v, \quad \varepsilon_z = \frac{\partial w}{\partial z}, \tag{11}$$

where u and w are the radial and axial displacement respectively. The FE discretization uses the dependent variables v and w, giving the stress gradient as:

$$\frac{\partial\sigma_z}{\partial r} = E\left[(1+\nu)(1-2\nu)(1-\nu)\frac{\partial^2 w}{\partial z\partial r} + \nu\left(\frac{\partial v}{\partial r} + r\frac{\partial^2 v}{\partial r^2} + 3\frac{\partial v}{\partial r}\right)\right]^{-1} \tag{12}$$

Generalized Neuber

Hoffmann and Seeger [8] extended the Neuber approach for general stress states by using equivalent stresses and strains, $\bar{\sigma}$ and $\bar{\varepsilon}$. In their formulation, Neuber's rule is

written: $\bar{\varepsilon}\bar{\sigma} = \bar{K}_t^2 \varepsilon_n^2 E$, where $\bar{K}_t$ is the equivalent stress concentration factor. Using the Mises yield criterion, $\bar{K}_t$ can be written in terms of elastic stress ratios for the principal stresses:

$$\bar{K}_t = \frac{K_t}{\sqrt{2}} \sqrt{(1-a^e)^2 + (1-b^e)^2 + (a^e - b^e)^2}\,, \quad a^e = \frac{\sigma_2^e}{\sigma_1^e}, \quad b^e = \frac{\sigma_3^e}{\sigma_1^e}, \tag{13}$$

where superscript *e* denotes elastic values of stress or strain. Equivalent notch stresses and strains can be related to principal notch stresses and strains by using Hencky's flow rule:

$$\varepsilon_i^p = \frac{3}{2} \frac{\bar{\varepsilon}^p}{\bar{\sigma}} \sigma_i\,, \tag{14}$$

where ε_i^p are the principal plastic strains, and the index *i* take the values 1,2 and 3. On a free surface, σ_3=0, and Eq. 14 can be expanded to:

$$\varepsilon_1 = \frac{\bar{\varepsilon}^p}{\bar{\sigma}}(\sigma_1 - \nu'\sigma_2), \quad \varepsilon_2 = \frac{\bar{\varepsilon}^p}{\bar{\sigma}}(\sigma_2 - \nu'\sigma_1), \quad \varepsilon_3 = \frac{\bar{\varepsilon}^p}{\bar{\sigma}}\nu'(\sigma_1 + \sigma_2)\,, \tag{15}$$

$$\nu' = \frac{1}{2} - \frac{\bar{\sigma}}{E\varepsilon}\left(\frac{1}{2} - \nu\right), \tag{16}$$

where ν is Poisson's ratio. Two additional equations are needed to solve this system of five unknowns. One is found from, the Mises yield criterion:

$$\bar{\sigma} = \frac{1}{\sqrt{2}} \sqrt{(\sigma_1 - \sigma_2)^2 + \sigma_1^2 + \sigma_2^2}\ . \tag{17}$$

The last equation is found by assuming that the elastic and plastic strain ratios are the same for both plastic and elastic solution:

$$\phi = \frac{\varepsilon_2}{\varepsilon_1} = \frac{\varepsilon_2^e}{\varepsilon_1^e}. \tag{18}$$

The solutions for the first principal stress and strain are:

$$\sigma_1 = \bar{\sigma}\frac{1}{\sqrt{1-a+a^2}}, \quad \varepsilon_1 = \bar{\varepsilon}\frac{1-\nu' a}{\sqrt{1-a+a^2}}, \quad a = \frac{\phi + \nu'}{1 + \nu'\phi} \tag{19}$$

Results

A very fine finite element mesh was needed to resolve the stresses and gradients at the notch root. The smallest element sizes were around 1 μm, creating a mesh in excess of 1 mill. degrees of freedom for each profile. The convergence was satisfactory for both the stress and gradient solution, although the latter showed discontinuities for subsurface solutions. The reason is that Eq. 12 is based on second derivatives of the dependent parameters, while the FE shape functions are quadratic. A small region was analyzed with cubic and quartic shape functions, but the gradient solution at the notch root did not change significantly.

The material parameter *c* in Eq. 9 was found for each specimen from the observed K_f and the calculated K_t for the notch *where the fatigue crack initiated*. A rather large scatter for *c*

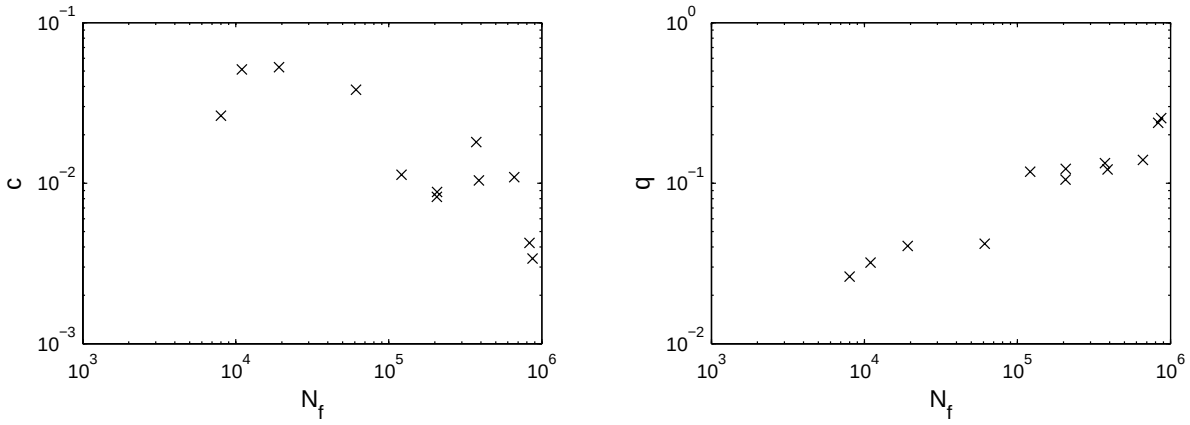

Figure 4: (Left) The material constant c from Eq. 9 vs. observed fatigue life.
(Right) Notch sensitivity q vs. fatigue life.

was observed, and as Figure 4 shows, there is a marked dependence on N_f. This is due to the commonly observed increasing notch sensitivity with increasing lives as shown in Figure 4.

Using the median value of c for all specimens, the strain amplitudes have been calculated with the Neuber and Hoffmann-Seeger correction for all the grooves where cracks initiated. As seen in Figure 5, the surface roughness reduces the fatigue life with a factor of about 10. The predicted values seem to have a steeper slope than the reference curve. The Hoffmann-Seeger correction predicts lower strains due to the higher constraints in the notch roots compared to a plane stress solution. The latter solution is therefore better, but cannot predict the correct strain outside the N_f region where c was extracted.

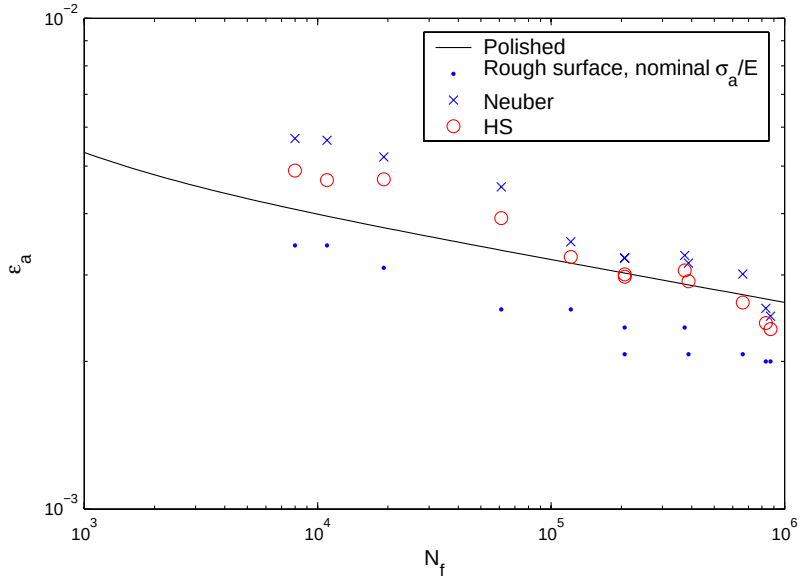

Figure 5: Comparison of the polished strain-life curve and the predicted strain amplitudes using the Neuber and Hoffmann-Seeger (HS)-correction using the median of c.

Subsurface axial stresses have been extracted for all major notches. In Figure 6 the stress ahead of the notch where failure initiated is shown as a bold line for two specimens with comparable stress gradients. The c parameter is however very different, as is the shape of the stress distribution ahead of the notch. As seen, the initiation site is not at the notch having the highest σ_z at the root , but at the notch that has the highest stress in the region 5-10 μm ahead of the notch. This was observed for all specimens, regardless of applied stress and K_t.

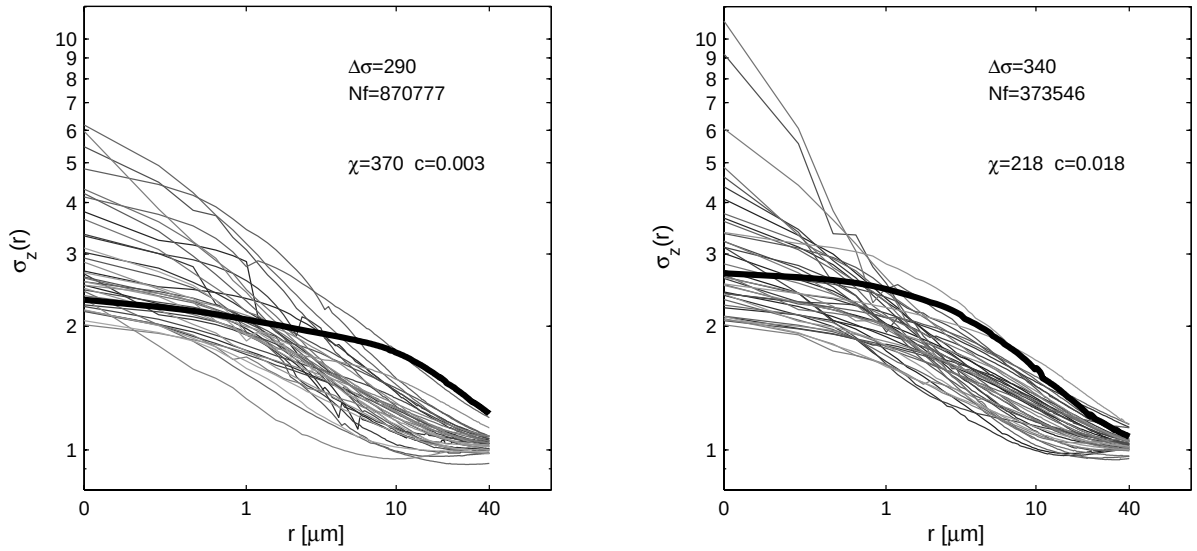

Figure 6: Axial stress at a distance *r* ahead of all major notch roots for two specimens. The bold lines indicate the stress solution for the notches where the cracks initiated.

Conclusion

The use of K_f was originally developed for the fatigue limit, giving the ratio of un-notched to notched endurance stresses. Klesnil and Lukáš [9] has linked K_f to the threshold stress intensity factor for small cracks using the length of non-propagating cracks, while Navarro et al [10] have used the mean half grain size. The latter theory is based on grain boundaries as obstacles to crack propagation, where the first boundary is assumed to be located a distance equal to half the grain size ahead of the notch. It is interesting to note that in the stress fields for the initiation sites (Figure 6), the stresses dominate over the other notches at a distance corresponding to half the grain size of about 10 μm. However, applying theories based on fatigue limit for the whole fatigue life does not seem appropriate.

Acknowledgements

This project is funded by The Research Council of Norway (The Industrial Manufacturing and Materials Conversion Program, VAREMAT).

References

1. H. Neuber, *Kerbspannungslehre*, Springer Verlag, 1958.
2. D. Arola and C. L. Williams. *Int. J. Fatigue*, vol. 24, 923-930, 2002.
3. R. Ohlsson et. al. *Machine Tools and Manufacture*, vol. 41, 1899-1907, 2001.
4. H. Neuber, *Konstruktion*, vol. 20, 245-, 1968.
5. R. E. Peterson, *Stress Concentration Factors*, John Wiley and Sons, New York, 1974.
6. S. K. Ås and B. Skallerud, In *Proc. 5th Int. Conf. on Low Cycle Fatigue*, Berlin, 2003.
7. E. Siebel and M. Stieler *Z. Ver. Deutch. Ing.*, 97-121, 1955.
8. M. Hoffmann and T. A. Seeger. *J. Eng. Mat. Tech.*, vol. 107, 250-260, 1985.
9. M. Klesnil and P. Lukáš, *Fatigue of Metallic Materials*, Elsevier, Amsterdam, 1992.
10. A. Navarro et al, In *Proc. Eng. Against Fatigue*, A.A. Balkema, Rotterdam, 1999.